Modelling neutron damage effects on tritium transport in tungsten

James Dark, Rémi Delaporte-Mathurin, Thomas Schwarz-Selinger, Etienne A Hodille, Jonathan Mougenot, Yann Charles, Christian Grisolia

OPEN ACCESS
IOP Publishing | International Atomic Energy Agency
Nuclear Fusion
Nucl. Fusion **64** (2024) 086026 (12pp)
https://doi.org/10.1088/1741-4326/ad56a0

Modelling neutron damage effects on tritium transport in tungsten

James Dark[1,2,*], Rémi Delaporte-Mathurin[3], Thomas Schwarz-Selinger[4], Etienne A. Hodille[1], Jonathan Mougenot[2], Yann Charles[2] and Christian Grisolia[1]

[1] CEA, IRFM/GCFPM, F-13108 Saint-Paul-lez-Durance, France
[2] Université Sorbonne Paris Nord, Laboratoire des Sciences des Procédés et des Matériaux, LSPM, CNRS, UPR 3407, F-93430 Villetaneuse, France
[3] Plasma Science and Fusion Center, Massachusetts Institute of Technology, Cambridge, MA 02139, United States of America
[4] Max-Planck-Insitut für Plasmaphysik, Bolstzmannstrasse 2, D-85748 Garching, Germany

E-mail: james.dark@cea.fr

Received 20 February 2024, revised 16 May 2024
Accepted for publication 11 June 2024
Published 24 June 2024

Abstract

A damage-induced hydrogen trap creation model is proposed, and parameters for tungsten are identified using experimental data. The methodology for obtaining these parameters using thermo-desorption analysis spectra data is outlined. Self-damaged and optionally annealed tungsten samples have undergone TDS analysis, which has been analysed to identify the properties of extrinsic traps induced by the damage and to determine how they evolve with damage and annealing temperature. A parametric study investigated the impact of the damage rate and temperature on tritium inventories in tungsten. Tritium transport simulations have been performed with FESTIM considering a 1D model of a 2 mm sample of tungsten with damage rates and temperatures varying from 0–10^2 dpa/fpy and 600–1300 K, respectively. The results show that after 24 h simultaneous exposure to neutron damage at 10^2 dpa/FPY and tritium implantation at 700 K, tritium inventories can increase by up to four orders of magnitude when damaged at a rate of 10^2 dpa/FPY compared to undamaged, defect-free tungsten, increasing further to five orders of magnitude after one full power year. The time taken to reach retention saturation shows the need for kinetic models of trapping properties on time scales relevant to reactor operation. The trap-creation model parameterisation procedure can be used to investigate neutron damage effects on other fusion-relevant materials such as EUROFER, Inconel and more.

Keywords: tungsten, neutron damage, annealing, trapping, tritium transport

(Some figures may appear in colour only in the online journal)

* Author to whom any correspondence should be addressed.

1. Introduction

Tungsten has been proposed as a suitable plasma-facing material due to its favourable thermal properties, resistance to irradiation and erosion effects [1]. Fusion power plants (FPP) are likely to utilise tungsten in components such as the divertor or the first wall in reactors such as ARC [2] and DEMO [3]. Accurate simulation of the hydrogen isotope transport is imperative to ensure safe operation and optimal performance of the FPP's using tritium. Furthermore, accurate simulations of subcomponents can better inform system-level fuel cycle models, potentially leading to better economic performances of an FPP [4, 5]. Tritium production in nuclear fusion devices presents a concern for designers due to its permeability through materials, and its radioactive nature requires accurate monitoring.

Tritium permeates through materials by diffusion. However, it can get trapped within microstructural defects such as vacancies, dislocations, interstitials, and voids. The properties of the traps are influenced by the density and distribution of the microstructural defects in the material and can significantly increase inventories within structural materials [6–8]. However, neutrons produced in the fusion plasma will damage plasma-facing components and reactor structural materials over the time of operation [9], altering the landscape of such microstructural defects. The irradiation environment and tritium production in a FPP will be characterised by the 14 MeV neutron radiation field, produced by the fusion reactions in the plasma [10]. It is expected that neutrons will damage components in DEMO and ARC at rates of 5 dpa/FPY and 20 dpa/FPY, respectively [2, 3]. Where dpa is the displacement per atom, and FPY represents the exposure during a Full Power Year operation. A thorough understanding and quantification of degradation in plasma-facing materials due to neutron damage will be needed for future fusion devices' safe and reliable operation. Many current experimental studies on damaged plasma-facing materials use ion irradiation to emulate aspects of neutron damage, as they can impart large damage doses comparatively quicker without specific safety concerns such as transmutation [12, 13]. One consequence of irradiation damage is the induction of additional microstructural defects [14]. Thus, as the microstructural defect landscape evolves with irradiation damage, so must the trap properties used to model them. The model was parameterised using data from heavy-ion irradiation instead of neutron irradiation data because there is no data on materials irradiated to levels expected in fusion reactors using neutrons. Although experimental studies indicate that hydrogen transport may differ under these conditions [15, 16], the model is assumed to represent the effects on hydrogen transport adequately. Additionally, increased tritium inventories will lead to higher levels of helium production as a result of decay [17].

Research shows that when materials experience neutron-like damage, they develop more defects. These extrinsic defects can trap hydrogen, potentially increasing inventories in the material [18, 19]. Although one might anticipate an increase in the density of hydrogen trapping sites with more neutron damage leading to more induced defects, research indicates that hydrogen retention reaches saturation after a certain level of damage [18, 20–23]. Subsequent damage dose does not affect hydrogen retention levels [24]. Typically, one can estimate hydrogen migration depth into a plasma-facing surface from the trapping properties of the material [8]. However, trap creation can mitigate migration, leading to higher concentrations of hydrogen close to the plasma-facing surface. This competition of regimes has been explored previously [25]. Furthermore, the presence of hydrogen isotopes within a material experiencing neutron-like damage has been shown to increase the rate of defect creation and mitigate the annealing of the traps created [26]. However, this phenomenon has not been considered in the present study.

A model is proposed to predict the temporal evolution of the damage-induced trap densities. A methodology is outlined to identify the model's parameters from thermo-desorption experiment data and deuterium depth profiling. The open-source hydrogen transport code FESTIM (v1.1.1) [27] was employed and extended to simulate tritium transport in tungsten with damage-induced traps.

All the results presented in this paper can be reproduced with the scripts available at [28].

2. Model parametrisation

2.1. Tritium transport governing equations

Tritium transport can be modelled using macroscopic rate equations first introduced by McNabb and Foster [29]:

$$\frac{\partial c_{\mathrm{m}}}{\partial t} = \nabla \cdot (D \nabla c_{\mathrm{m}}) + S - \sum \frac{\partial c_{\mathrm{t},i}}{\partial t} \tag{1}$$

$$\frac{\partial c_{\mathrm{t},i}}{\partial t} = \nu_{\mathrm{t},i} \cdot c_{\mathrm{m}} \cdot (n_i - c_{\mathrm{t},i}) - \nu_{\mathrm{dt},i} \cdot c_{\mathrm{t},i}. \tag{2}$$

Equations (1) and (2) describe the thermo-kinetic model used for tritium transport. The concentration of tritium c is comprised of the mobile concentration c_{m} and the total trapped concentration $\sum c_{\mathrm{t},i}$. The first term on the right-hand side of equation (1), $\nabla \cdot (D \nabla c_{\mathrm{m}})$, is a Fickian diffusion term characterised by the diffusion coefficient, $D = D_0 \cdot \exp(-E_{\mathrm{diff}}/(k_B \cdot T)$ in units $[\mathrm{m}^2 \cdot \mathrm{s}^{-1}]$ and $k_B = 8.617 \times 10^{-5}\,\mathrm{eV \cdot K}^{-1}$ is the Boltzmann constant. S is the volumetric source term of mobile hydrogen in $[\mathrm{m}^{-3} \cdot \mathrm{s}^{-1}]$, used to model plasma implantation. The exchange between the mobile (c_{m} in (m^{-3})) and trapped ($c_{\mathrm{t},i}$ in (m^{-3})) particle concentrations is described by $\sum \frac{\partial c_{\mathrm{t},i}}{\partial t}$. The trap density, n_i, is in units (m^{-3}). $\nu_{\mathrm{t},i} = \nu_{\mathrm{t},0} \cdot \exp(-E_{\mathrm{t},i}/(k_{\mathrm{B}} \cdot T)$ and $\nu_{\mathrm{dt},i} = \nu_{\mathrm{dt},0} \cdot \exp(-E_{\mathrm{dt},i}/(k_{\mathrm{B}} \cdot T))$ are the trapping and de-trapping rates in $[\mathrm{m}^3 \cdot \mathrm{s}^{-1}]$ and (s^{-1}) respectively. $E_{\mathrm{t},i}$ is equal to diffusion activation energy, E_{diff}. $E_{\mathrm{dt},i}$ is the de-trapping energy, equivalent to the sum of the binding energy and the diffusion activation energy.

The trap density, n_i, typically does not evolve in time or vary spatially for a given material. However, this work explores the

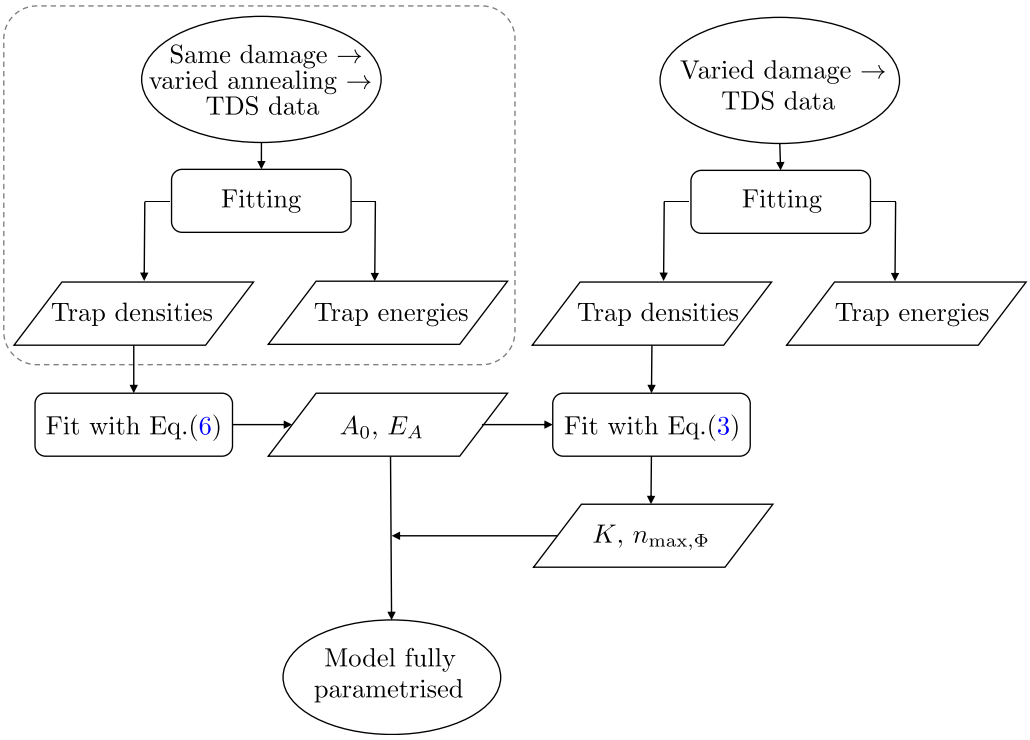

Figure 1. Process diagram for evaluating variables in equation (3). Work completed by Pečovnik *et al* [11] is highlighted in the dashed box.

impact of this parameter varying due to irradiation damage and annealing effects.

2.2. Damaged induced trap model definition

$$\frac{\partial n_i}{\partial t} = \Phi \cdot K\left[1 - \frac{n_i}{n_{\mathrm{max},\Phi}}\right] - A \cdot n_i. \tag{3}$$

Equation (3) describes the temporal evolution of trap density n_i. The creation term, $\Phi \cdot K[1 - \frac{n_i}{n_{\mathrm{max},\Phi}}]$, describes the number of traps formed by damage to a given saturation point $n_{\mathrm{max},\Phi}$. Φ is the damage rate in [dpa·s^{-1}], and can vary spatially. K is the trap creation factor in [traps·m^{-3}·dpa^{-1}]. Similar models have already been used to simulate trap creation during self-damaging in W [21, 25]. However, these models do not account for possible annealing of the traps. A is the trap annealing factor in (s^{-1}) and is described as an Arrhenius law where $A = A_0 \cdot \exp(-E_A/(k_\mathrm{B} \cdot T))$. This was chosen as similar models have been implemented to model the annealing of defects induced by plastic deformation [30]. A methodology is outlined for fitting the parameters of such a model from experimental results with damaged tungsten samples (see figure 1). TDS results can be used to identify the hydrogen trapping parameters of a material. Furthermore, how such results change with levels of damage and annealing temperature can illuminate how the trap properties depend on such factors.

Two experimental data sets were used to evaluate the unknown parameters in equation (3). Data from the work of Pečovnik *et al* [11] has been used to evaluate the annealing parameters (A_0 and E_A). To evaluate the damaging parameters (K and $n_{\mathrm{max},\Phi}$), unpublished data from T. Schwarz–Selinger was used that was generated following the procedure outlined in [31].

2.3. Model assumptions

To account for the instantaneous hydrogen detrapping when a trap is annealed, a sink term $A_i \cdot c_{\mathrm{t},i}$ is added to equation (2).

$$\frac{\partial c_{\mathrm{t},i}}{\partial t} = \nu_\mathrm{t} \cdot c_\mathrm{m} \cdot (n_i - c_{\mathrm{t},i}) - \nu_\mathrm{dt} \cdot c_{\mathrm{t},i} - A_i \cdot c_{\mathrm{t},i}. \tag{4}$$

It is assumed that only empty traps are created and trapped hydrogen, $c_{\mathrm{t},i}$, released from annealed traps, is not re-trapped, contributing to the mobile concentration, c_m. This is due to a current technical limitation of the FESTIM code, which would require an additional governing equation to explicitly model the empty trapping sites. However, this feature will be integrated into a future version of the code. It is also assumed that filled and empty traps anneal at the same rate, A. The derivation of this sink term is outlined in the appendix. Furthermore, it is assumed that the damage rate does not influence the model's kinetics and that traps induced by damage cannot diffuse.

2.4. Annealing parameter estimation

In a case in which samples are irradiated, then annealed, one can simplify equation (3) to model the latter stage, as no damaging takes place thus the damage rate Φ is equal to zero and equation (3) can be reduced to:

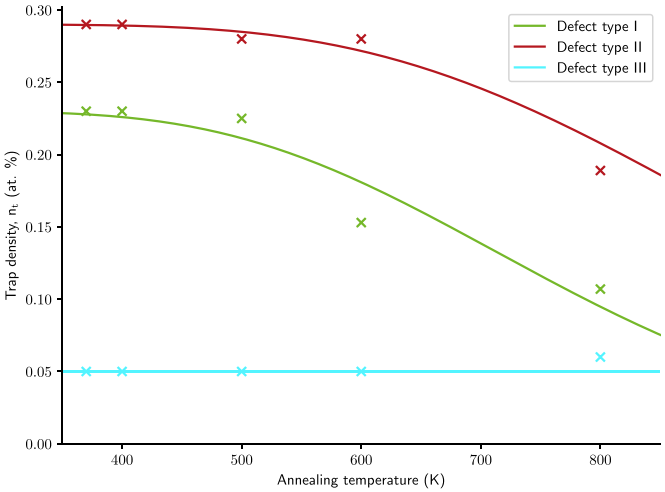

Figure 2. Trap densities evolution with annealing temperature fitted using equation (6). Experimental data points [11].

Table 1. Annealing parameter values for each defect type.

Defect type	A_0 (s^{-1})	E_A (eV)
I	6.18×10^{-3}	0.24
II	6.18×10^{-3}	0.30
III	0	—

$$\frac{\partial n_i}{\partial t} = -A \cdot n_i. \tag{5}$$

Solving this equation analytically, the trap density is expressed as:

$$n_i = n_{i,0} \cdot \exp\left(-A \cdot \Delta t\right) \tag{6}$$

where $n_{i,0}$ is the initial trap concentration (no annealing) and Δt is the annealing time. From this, one can fit the results from Pečovnik *et al* [11] with equation (6), using $\Delta t = 2h$, allowing for the identification of the two unknown parameters (A_0 and E_A) from equation (3). These values can then identify the remaining unknown trap creation parameters. This is detailed in section 2.4. The first factor evaluated from equation (3) was the trap annealing factor A. Three types of defects were identified in the work of Pečovnik *et al* [11], and the trap densities evaluated for each defect type were used. Each trap's density variation with annealing temperature is fitted using equation (6) (see figure 2). Each trap type was fitted to obtain values of A_0 and E_A, the values of which are outlined in table 1. Defect type III has been incorporated into the model based on the assumption that it is resistant to annealing. This assumption is supported by findings in the experimental literature [32], which suggest that certain defects either cannot undergo annealing or require significantly higher temperatures.

It is important to note that the data for fitting the model was derived from tungsten samples pre-loaded with deuterium before irradiation. The impact of the presence of deuterium in a sample on defects in tungsten during irradiation is an ongoing area of research [20, 25, 33]. While other studies have explored the influence of annealing temperature on tungsten samples damaged without the presence of deuterium [23, 26], it has been undertaken with low energy atom exposure at high temperature (500 K) preventing defect I from being filled with D. Thus, annealing data for this defect is not available from these studies. In addition, it could be argued that including deuterium during the damaging process better represents components in an operational reactor. Consequently, the pre-loaded damaged samples are employed to analyse annealing parameters.

The values obtained from this parameter estimation procedure are then utilised in the subsequent section to assess trap creation parameters.

2.5. Trap creation parameter estimation

To evaluate the trap creation parameters, K and $n_{\max,\Phi}$, a similar approach was used as in section 2.4. T. Schwarz-Selinger conducted an experimental campaign in which samples of self-damaged tungsten underwent ion beam analysis and TDS to evaluate how damage affects deuterium retention. In the study, recrystallised polycrystalline tungsten (PCW) samples (2000 K Plansee 99.97 at.%, 10–50 μm grain size) were exposed to 20 MeV W^{6+} ions at 800 K for varying exposure times. Following this, the samples were exposed to a 15 eV/D with a flux of 6×10^{19} D·m^{-2}·s^{-1} for a total fluence of 10^{25} D·m^{-2} at a temperature of 370 K. The samples were analysed using TDS with a heating ramp of 0.05 K·s^{-1}. For the damaging parameters, TDS data from seven damaged tungsten samples (0.001–2.5 dpa) were analysed to provide damage-induced trap properties. The TDS data for each sample was fitted to provide the detrapping energies and densities for traps induced by damage. The fitting was undertaken with the constraint that each TDS spectrum must have the same number of traps with the same de-trapping energies. From this, one evaluates how the trap density varies with damage for each induced trap. The results of the TDS data fittings can identify the remaining unknown parameters (K and $n_{\max,\Phi}$) from equation (3). From this, the model is characterised for each damaged-induced trap and can be modelled using FESTIM to investigate the influence of damaged-induced traps on tritium transport in tungsten. Section 2.5 outlines the experimental data and parameter fitting details. A diagram is shown in figure 1, which visually outlines the parameter evaluation process. Modelling the experimental set-up using SRIM identified the damage profile produced by the ions and peak levels of damage at 0.001, 0.005, 0.023, 0.1, 0.23, 0.5 and 2.5 dpa, excluding one that was not damaged [34]. The damage occurred within the sample's first 2–3 μm; thus, damage-induced trap creation would only happen in the same area. To account for this, the induced traps were modelled using a Fermi–Dirac density distribution (see figure 3). The deuterium depth profiles measured with ^{3}He nuclear reaction analysis can be well described with these Fermi–Dirac distributions.

$$f(x) = \frac{1}{1 + \exp\left(\dfrac{x - x_0}{\Delta x_0}\right)} \tag{7}$$

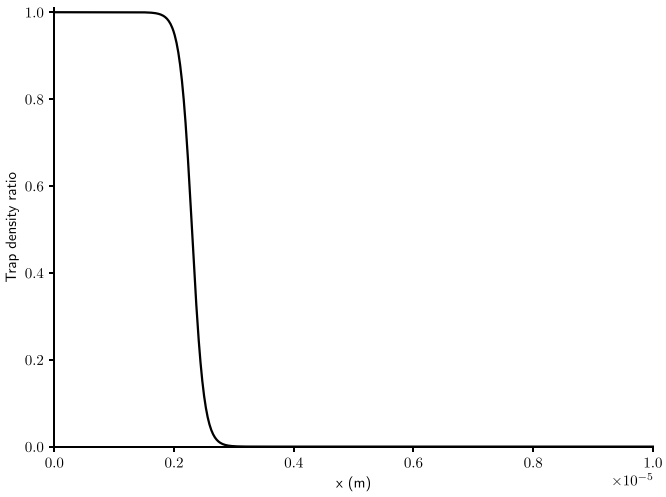

Figure 3. Trapping site density Fermi–Dirac distribution described by equation (7).

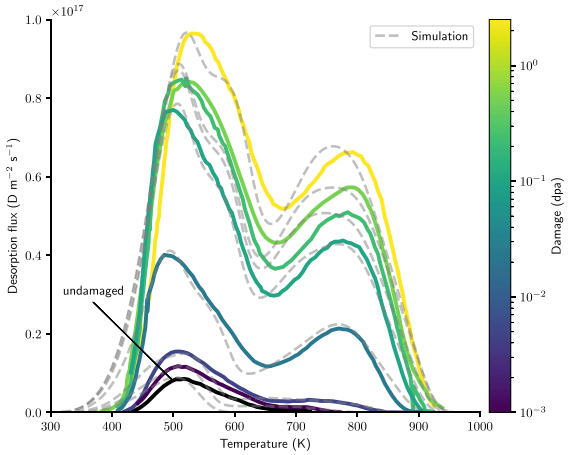

(a) Results of TDS analysis from tungsten samples damaged to various levels (0.001 - 2.5 dpa at 800 K and decorated with D at 370 K

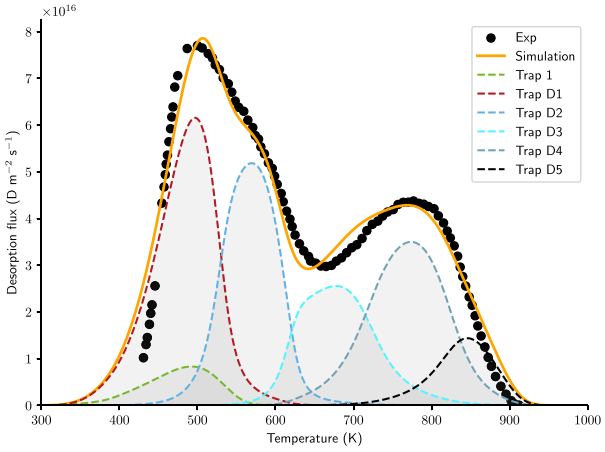

(b) TDS data for tungsten sample damaged to 0.1 dpa, fitted using one intrinsic trap and four extrinsic traps

Figure 4. TDS data with fittings (*a*) and highlighted fitting of the 0.1 dpa case (*b*).

where $x_0 = 2.3\ \mu$m and $\Delta x_0 = 0.1\ \mu$m.

The TDS procedure of the 8×10^{-04} m-thick tungsten sample was simulated in 1D using FESTIM. The pre-exponential factor of the diffusion coefficient of deuterium in tungsten was $D_0 = 1.6 \times 10^{-7}\,\mathrm{m^2{\cdot}s^{-1}}$ and its activation energy $E_\mathrm{D} = 0.28\,\mathrm{eV}$ [35]. The procedure consists of three phases: implantation, resting, and desorption. For all phases, a homogeneous Dirichlet boundary condition (i.e. $c_\mathrm{m} = 0$) is applied to both boundaries of the 1D model, equivalent to instantaneous recombination. For the implantation phase, the source term in equation (1) is $S = \Gamma \cdot f(x)$, where Γ is the implanted ion flux in $[\mathrm{m^2 \cdot s^{-1}}]$ and $f(x)$ is a Gaussian distribution with R_p as its mean value and σ its width, the values of which have been determined using SRIM [34] and are outlined in table 2. This phase lasts t_imp and has a uniform temperature of T_imp. The second phase is the resting period in which no implantation is occurring and has a uniform temperature of T_rest for t_rest. The final phase models the desorption due to a linear uniform temperature increase with a given ramp β. Table 2 gives the TDS simulations' parameters. The TDS fitting procedure is the same as used by Delaporte-Mathurin *et al* [36].

Initially, the data from the un-damaged sample was analysed. This was to identify any intrinsic traps, which can then be used for modelling the damaged samples. A single trap fits the TDS with an associated de-trapping energy of 1.04 eV (see table 3). The TDS spectra from the damaged samples were then fitted considering the intrinsic trap previously identified in the whole sample and any further extrinsic traps with the distribution described by equation (7).

Five extrinsic traps were used to fit the TDS data with detrapping energies of 1.15, 1.35, 1.65, 1.85 and 2.05 eV, and are hereafter referred as D1, D2, D3, D4 and D5, respectively (see table 4 and figure 5).

The literature on atomistic scale modelling can illuminate the specific types of defects that may be responsible for traps D1-5. According to simulations of collision cascades in tungsten, self-interstitial atom (SIA) clusters are the primary defect resulting from irradiation, along with the creation of monovacancies, dislocation loops and voids [13]. However, density functional theory (DFT) calculations show the detrapping energy of deuterium with SIA clusters is typically below $E_\mathrm{dt} = 0.95\,\mathrm{eV}$ [37]. Consequently, since the deuterium was implanted at 370 K, these defects do not effectively retain the deuterium, as evidenced by the thermal desorption

Table 2. TDS simulation parameters.

Property	Value	Unit
T_imp	370	K
T_rest	295	K
Γ	1×10^{20}	$\mathrm{m^{-2} \cdot s^{-1}}$
R_p	0.7	nm
gma	0.5	nm
t_imp	72	h
t_rest	12	h
β	0.05	$\mathrm{K{\cdot}s^{-1}}$

Table 3. Fitted intrinsic trap properties.

Property	Value	Unit
E_t	0.28	eV
$\nu_{t,0}$	7.77×10^{-17}	$m^3 \cdot s^{-1}$
E_{dt}	1.04	eV
$\nu_{dt,0}$	1.0×10^{13}	s^{-1}
n_i	2.4×10^{22}	m^{-3}

Table 4. Results of the model parametrisation for the damage-induced traps.

Trap	E_{dt} (eV)	K [traps·m^{-3}·dpa^{-1}]	$n_{max,\Phi}$ (m^{-3})	A_0 (s^{-1})	E_A (eV)
D1	1.15	9.0×10^{26}	6.9×10^{25}	6.18×10^{-3}	0.24
D2	1.35	4.2×10^{26}	7.0×10^{25}	6.18×10^{-3}	0.24
D3	1.65	2.5×10^{26}	6.0×10^{25}	6.18×10^{-3}	0.30
D4	1.85	5.0×10^{26}	4.7×10^{25}	6.18×10^{-3}	0.30
D5	2.05	1.0×10^{26}	2.0×10^{25}	0	—

spectroscopy (TDS) data. Detrapping energies of deuterium from monovacancies typically range between 1.0 and 1.4 eV [38, 39], consistent with traps D1 and D2 (characterised by desorption around 500–600 K in figure 2). Monovacancies were also identified as defect type I in the work of [11]. Similarly detrapping energies of deuterium from vacancy clusters (up to size 20) fall between 1.6 and 1.9 eV [40], aligning with the traps D3 and D4 (characterised by desorption around 750–850 K in figure 2). Vacancy clusters are the defect type II identified in the work of [11]. Furthermore, DFT calculations suggest that the barrier from the surface to bulk, which can emulate large vacancy clusters, is also around 2.0 eV [39, 41, 42], coherent with trap D5. Large vacancy clusters were identified as defect type III in the work of [11]. The traps identified are also in agreement with previous rate equation simulations done on similar systems [11, 13, 19, 43–45].

Using atomistic modelling studies as a reference, we can make informed guesses about the features of a trap. However, the energy required to release a trapped particle does not always reflect the trap's size. Large vacancies in a lattice can accommodate multiple hydrogen atoms. According to atomistic modelling, when multiple atoms are trapped within the same defect, the dynamics of their release can cause variations, leading to distinct peaks in TDS results linked to different traps [40].

Beyond 1300 K, recrystallisation effects are more prominent in tungsten, which will alter the microstructural defect landscape [46, 47]. Furthermore, the increased mobility of vacancy clusters at such high temperatures can produce larger ones [48, 49]. Thus, to ensure the model conforms beyond 1300 K, more experimental data is required. Another issue with the presented methodology is the same as other inverse problem-solving methods. As shown previously [50], one can fit the same TDS data using multiple sets of parameters, meaning various solutions to the same optimisation problem exist. Additionally, the data has been collected from

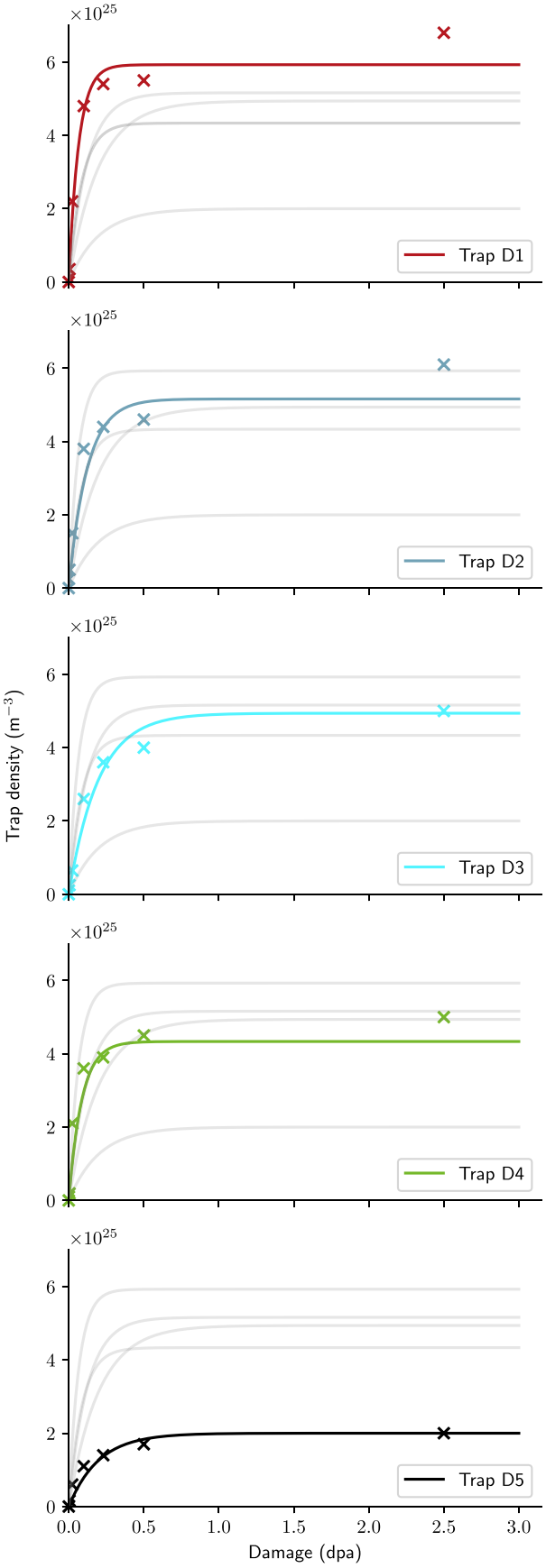

Figure 5. Trap concentrations with increasing damage dose from the fitted TDS, then fitted using the current model.

self-damaging experiments (W6+ ions), not 14 MeV neutron damage. Neutron damage will create a more uniform damage profile across the sample than self-damage. Furthermore, the defects of self-damaging ions are likely different from those characterised by fast neutrons. Hence, TDS analysis would potentially render different results, changing the parameters for this model. TDS spectra obtained on W damaged with fission-generated neutrons show similar high-temperature peaks as the ones shown here for self-damaged W. TMAP analyses of these neutron-damaged W show similar detrapping energies [45]. Thus, the nature of the identified defect in self-damaged W is relevant to neutron-damaged W; only the distribution (meaning the trap concentration) may differ.

Nevertheless, the evaluated trap properties are taken forward to model the influence of damage-induced traps on tritium retention levels in tungsten within tokamak-like environmental conditions.

3. Impact on trap concentration and tritium inventories

To investigate the potential significance of the damage-induced trap densities evaluated in section 2.5, equation (3) was solved numerically to evaluate how the total trap density varies with damage rate. A scenario is considered in which 2 mm of tungsten is damaged homogeneously (emulating a likely neutron damage profile in the first wall of a fusion reactor) [51]. It should be noted that the model was parameterised using heavy-ion irradiation data, which affects only the first few micrometres of a sample; it is assumed that similar damage characteristics apply throughout the sample when it is subjected to neutron damage. Primarily, two cases are considered with constant temperatures of 295 K and 800 K, varying the damage rate, Φ, from 10^{-3} to 10^{3} dpa/FPY and ran over a FPY (see figure 6).

3.1. Trap concentration evolution

Including the annealing term A in equation (3) affects the dynamics of trap creation. Although, as the rate of damage increases, the ratio of $\Phi \cdot K$ to A increases significantly, trap creation becomes independent of annealing (see figure 6). Additionally, when the ratio of $\Phi \cdot K$ to $n_{\max,\Phi}$ exceeds A, the characteristic time is approximately $\frac{n_{\max,\Phi}}{\Phi \cdot K}$. Given that K is large, the characteristic time becomes shorter, which explains why the curves overlap at high damage rates.

Notably, in the case of DEMO, where the highest level of damage is anticipated to be 5 dpa/FPY [3], and in ARC with a damage level of 20 dpa/FPY [2], the temperature continues to exert an influence. However, it is crucial to highlight that temperature applies its most substantial and noteworthy effect at the lower levels of damage. For damage rates anticipated in DEMO and ARC, the disparity in trap density is approximately a factor of four, contingent upon temperature variations. In particular, at the lowest levels of damage, specifically at 10^{-3} dpa/FPY, the contrast becomes markedly pronounced, escalating to a substantial factor of 50. This exponential increase in the difference underscores the heightened sensitivity of trap density to temperature at lower damage levels, revealing a nuanced relationship that merits careful consideration in analysing materials under irradiation.

3.2. Tritium retention

The hydrogen transport code FESTIM (v1.1.1) was employed to evaluate the influence of damage-induced traps on tungsten tritium retention levels. Simulations of a 2 mm W slab at a constant temperature of 700 K show the impact of damage-induced traps on tritium retention over time and migration after 24 h (see figure 7). The 1D model consists of a plasma-implantation and reflective boundary conditions on the left and right sides of the domain, respectively. Implantation of tritium from the plasma was modelled (see equation (8)) where φ_{imp} is the implanted flux in $[\text{m}^2 \cdot \text{s}^{-1}]$ and R_p is the implantation depth expressed in [m]. This boundary condition allows for modelling an implanted source in high flux and high-temperature conditions without needing a nanometre-scale mesh as done in [52],

$$c_{\text{m}} = \frac{\varphi_{\text{imp}} R_p}{D} \tag{8}$$

The implantation flux used was 10^{20} $\text{m}^{-2}\cdot\text{s}^{-1}$ with an assumed implantation depth of 9 mm. The diffusion coefficient of hydrogen [35] has been scaled by a factor $1/\sqrt{3}$ to emulate tritium [53]. The complete scripts for the FESTIM model are available on the accompanying GitHub repository [28].

The results of the transient simulations are shown in figure 7). The upper figure illustrates how the tritium inventories vary for different levels of damage in the tungsten model. The undamaged case is shown to reach a point of saturation after 10^3 s. Notably, after 24 h, tungsten damaged at a rate of 10^2 dpa/FPY has an inventory four orders of magnitude higher compared to the undamaged case, and after a full power year, this escalation intensifies further to five orders of magnitude after 1 FPY. In cases with a lower damage rate, tritium can migrate from the plasma source on the left side through the entire domain. Despite significantly higher inventories in cases with substantial damage rates, tritium migration is mitigated; this inventory is confined within the initial 0.1 mm of tungsten in scenarios with the most significant damage rate at 10^2 dpa/FPY (see figure 7). Furthermore, it can be seen that even in the lowest damage rate, the tritium inventory is yet to reach a point of saturation after 1 FPY. Moreover, the level of tritium retention in the lowest rate of damage (10^{-5} dpa/FPY) is shown to follow the same behaviour as the undamaged case, up till beyond 10^5 s, at which point the tritium has migrated through the whole sample. Still, the traps continue to be formed; thus, the retention across the whole sample increases. This shows the competition between two regimes at play: trap creation and tritium migration. The tritium migration regime (at a high dpa rate) occurs when the

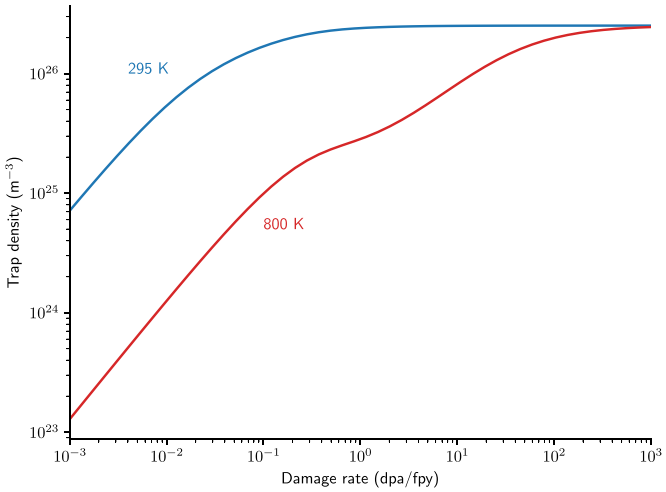

Figure 6. Total trap densities at 295 K and 800 K with variation in the damage rate after one FPY.

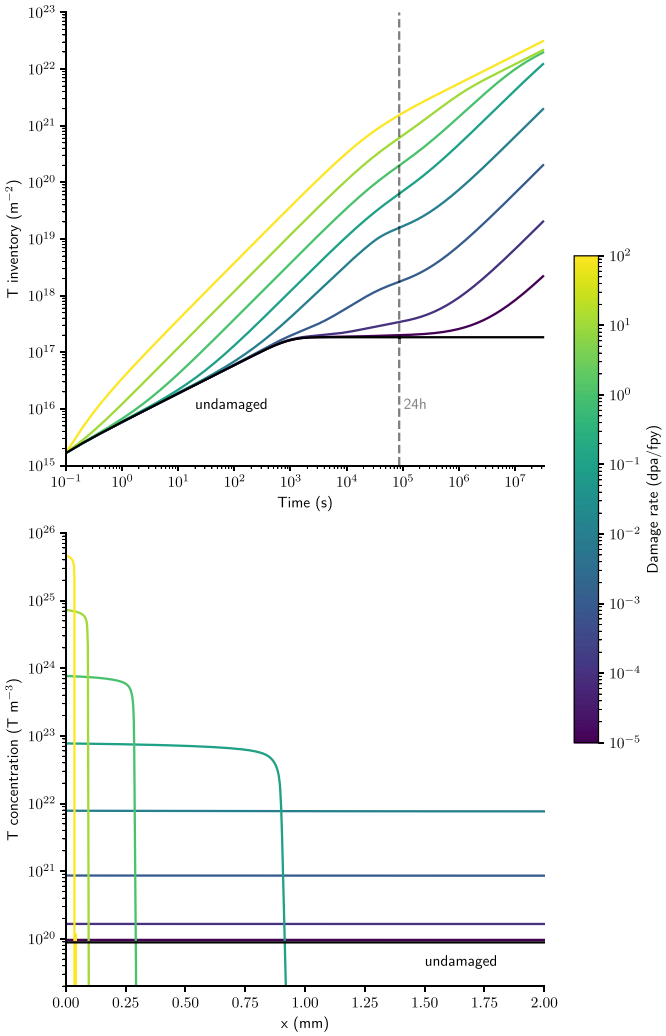

Figure 7. Tritium inventory over 1 FPY (top) per unit section and the concentration distribution after 24 h (bottom) from simultaneous damage exposure and tritium implantation, at 700 K varying the damage rate.

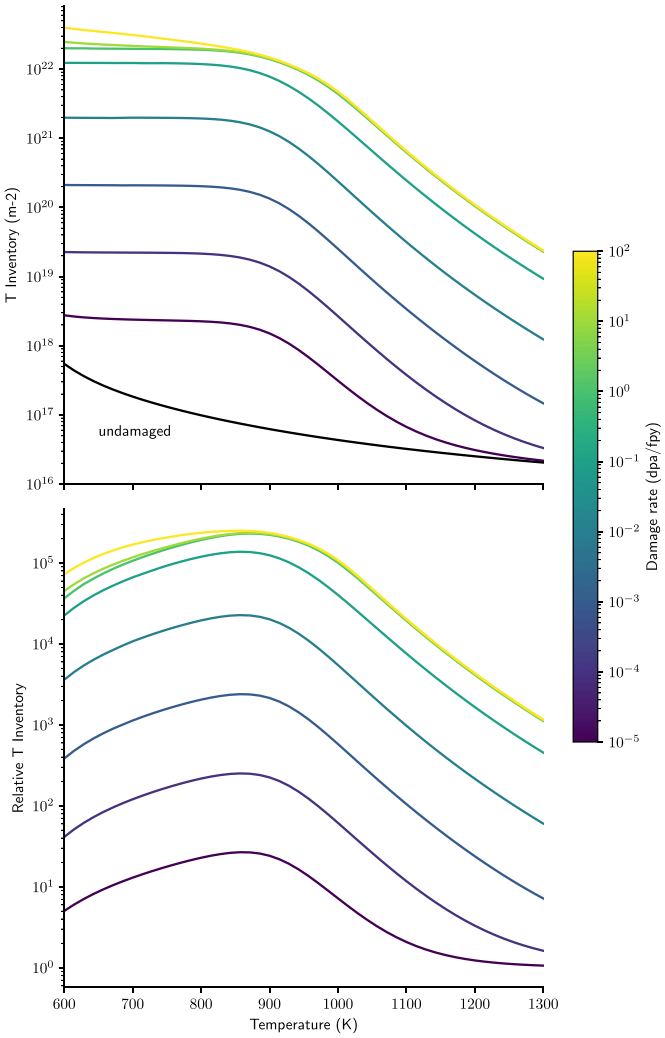

Figure 8. Tritium inventory in tungsten in varying damaged cases per unit section, relative to an undamaged case, after 1 FPY varying temperature.

trap concentration saturates quickly, and the tritium inventory is limited by tritium migration from the surface to the bulk (left to right on figure 7). The trap creation regime (low dpa rate) occurs when the tritium quickly migrates through the W slab, and the tritium inventory is limited by the trap creation build-up (the tritium concentration goes from bottom to top in figure 7). Tritium migration has been studied extensively, and work in the literature shows how the migration depth can be predicted depending on the trap properties considered [54]. However, this model does not account for a temporally evolving trap density term. The relation between trap creation and tritium migration has been explored in similar work in the literature, in which the same behaviour is observed [11].

Expanding the scope of the analysis to include variations in both sample temperature and damage rate reveals the impact of damage-induced traps on tritium retention levels after one FPY depends on both factors (see upper figure 8). In the undamaged case, a near-standard Arrhenius law is observed with the tritium retention after one FPY with temperature variation. Two distinct behaviours are observed in tritium retention levels. Below 900 K, the retention levels are shown to be temperature independent, as the tritium implanted gets trapped in the damage-induced defects. However, the tritium has enough energy to escape the traps beyond this temperature. With higher temperatures, more tritium can be de-trapped, reducing the inventory and levels approach the standard undamaged case. The damage rate exacerbates the retention level, although following the same two behaviours in each case. Although the highest magnitude of tritium retention occurs at the lowest temperatures, the highest value relative to the undamaged case occurs around 850 K. Around this value, the temperature is high enough to detrap any tritium within the intrinsic trap of the sample but not high enough to remove any tritium from the damage-induced traps (see lower figure 8). This result could be of particular concern for fusion devices, as this temperature range is within the operational limitations of tungsten.

4. Conclusion

This work presents a new mathematical model for describing hydrogen traps induced by displacement damage in tungsten, including trap creation and annealing. The methodology to parameterise the model is detailed, allowing its direct application to other materials of interest. TDS data from damaged samples annealed at various temperatures have been analysed and fitted to obtain the annealing parameters for the presented model. TDS data from deuterium-loaded tungsten samples displacement damaged to different doses at 800 K has also been fitted, from which five extrinsic traps were identified. The associated trap density evolution with damage level was used to obtain trap creation parameters for the presented model. With the model parameterised, FESTIM was employed to investigate the potential significance of such damaged-induced traps on tritium transport in tungsten.

Transient inventory results have shown that, after 24 h of exposure to damage at a rate of 10^2 dpa/FPY and tritium implantation at 700 K, inventories may increase by four orders of magnitude. Furthermore, the difference in the trap creation rate compared to the trapping rate results in localised inventory build-ups closest to the tritium source. After one FPY, results show that tritium inventories may increase by more than five orders of magnitude when considering damage-induced trapping effects. The highest relative inventories compared to an undamaged case occur around 850–900 K with inventories five orders of magnitude higher than an undamaged case at damage rates of 10^2 dpa/FPY. Tritium inventories are shown not to reach a point of saturation after a FPY transient, highlighting the importance of kinetic models to

describe the influence of neutron damage on tritium inventories. This refined understanding of the intricate dynamics in tritium retention and migration, influenced by varying damage rates and temperatures, contributes significantly to comprehending tungsten's behaviour in fusion reactor scenarios.

The model presented has been parameterised using data from ion-damaged samples, which have been shown to emulate aspects of neutron damage [12]. However, data from samples irradiated with neutrons with fusion-relevant energies and fluxes will be needed to improve the model's reliability. Facilities such as IFMIF-DONES [55], which will be a powerful neutron irradiation facility planned as part of the EUROfusion roadmap, will allow for the study and qualification of materials to be exposed to the DEMO plasma. Furthermore, the model can be developed further to account for hydrogen stabilisation effects on trap creation and annealing.

The presented results show that neutron damage-induced traps can significantly affect tritium transport in tungsten. Regarding safety, a higher quantity of the radioactive tritium may be trapped in components using a tungsten first wall. Economically, a higher trapped inventory means less of the tritium produced by the breeding blanket can be recovered, meaning a higher startup inventory and larger tritium breeding ratio will be required for the same tritium doubling time [4]. Furthermore, larger tritium inventories will produce more helium through decay, resulting in more bubble formation, contributing to embrittlement effects, and reducing the lifespan of the plasma-facing components. Thus, the influence of damage-induced trapping in tritium transport modelling should be considered, and the same work should be applied to other structural materials such as EUROfer.

Acknowledgments

This work has been carried out within the framework of the EUROfusion Consortium, funded by the European Union via the Euratom Research and Training Programme (Grant Agreement No 101052200—EUROfusion). Views and opinions expressed are however those of the author(s) only and do not necessarily reflect those of the European Union or the European Commission. Neither the European Union nor the European Commission can be held responsible for them.

Appendix

When a trap is annihilated, atoms trapped in it are instantaneously released as mobile ones. For a population of traps with a density n_i, the concentration rate of trapped atoms released by annihilation can be expressed as $\dot{c}_{t,i}^{\text{release}} = \theta_{t,i}\dot{n}_i$, where $\theta_{t,i}$ represents the trap occupancy (equal to $c_{t,i}/n_i$) and $\dot{n}_i = -An_i$ the annihilation rate.

This release has to be accounted for in the chemical balance equations of both c_m and $c_{t,i}$:

$$\begin{cases} \frac{\partial c_{\text{m}}}{\partial t} = \nabla \cdot (D\nabla c_{\text{m}}) + S - \sum \frac{\partial c_{\text{t},i}^{r}}{\partial t} + \sum \dot{c}_{t,i}^{\text{release}} \\ \frac{\partial c_{\text{t},i}}{\partial t} = \frac{\partial c_{\text{t},i}^{r}}{\partial t} - \dot{c}_{t,i}^{\text{release}} \\ \frac{\partial c_{\text{t},i}^{r}}{\partial t} = \nu_{\text{t}} \cdot c_{\text{m}} \cdot (n_i - c_{\text{t},i}) - \nu_{\text{dt}} \cdot c_{\text{t},i} \\ \dot{c}_{t,i}^{\text{release}} = \theta_{t,i}\dot{n}_i = -Ac_{t,i} \end{cases} \tag{9}$$

that can be rewritten as

$$\begin{cases} \frac{\partial c_{\text{m}}}{\partial t} = \nabla \cdot (D\nabla c_{\text{m}}) + S - \sum \frac{\partial c_{\text{t},i}}{\partial t} \\ \frac{\partial c_{\text{t},i}}{\partial t} = \nu_{\text{t}} \cdot c_{\text{m}} \cdot (n_i - c_{\text{t},i}) - \nu_{\text{dt}} \cdot c_{\text{t},i} - Ac_{\text{t},i} \end{cases} \tag{10}$$

ORCID iDs

James Dark https://orcid.org/0000-0002-0456-7210
Rémi Delaporte-Mathurin https://orcid.org/0000-0003-1064-8882
Thomas Schwarz-Selinger https://orcid.org/0000-0001-7461-2817
Etienne A. Hodille https://orcid.org/0000-0002-0859-390X
Jonathan Mougenot https://orcid.org/0000-0001-7397-0102

References

[1] Philipps V. 2011 Tungsten as material for plasma-facing components in fusion devices *J. Nucl. Mater.* **415** S2–S9
[2] Sorbom B.N. *et al* 2015 ARC: a compact, high-field, fusion nuclear science facility and demonstration power plant with demountable magnets *Fusion Eng. Des.* **100** 378–405
[3] Federici G., Biel W., Gilbert M.R., Kemp R., Taylor N. and Wenninger R. 2017 European DEMO design strategy and consequences for materials *Nucl. Fusion* **57** 092002
[4] Meschini S. Ferry S.E., Delaporte-Mathurin R. and Whyte D.G. 2023 Modeling and analysis of the tritium fuel cycle for ARC- and STEP-class D-T fusion power plants *Nucl. Fusion* **63** 126005
[5] Coleman M., Hörstensmeyer Y. and Cismondi F. 2019 DEMO tritium fuel cycle: performance, parameter explorations and design space constraints *Fusion Eng. Des.* **141** 79–90
[6] Dark J., Delaporte-Mathurin R., Charles Y., Hodille E.A., Grisolia C. and Mougenot J. 2021 Influence of hydrogen trapping on WCLL breeding blanket performances *Nucl. Fusion* **61** 116076
[7] Delaporte-Mathurin R. *et al* 2021 Fuel retention in WEST and ITER divertors based on FESTIM monoblock simulations *Nucl. Fusion* **61** 126001
[8] Hodille E.A., Bonnin X., Bisson R., Angot T., Becquart C.S., Layet J.M. and Grisolia C. 2015 Macroscopic rate equation modeling of trapping/detrapping of hydrogen isotopes in tungsten materials *J. Nucl. Mater.* **467** 424–31
[9] Barabash V., Federici G., Rödig M., Snead L.L. and Wu C.H. 2000 Neutron irradiation effects on plasma facing materials *J. Nucl. Mater.* **283–287** 138–46

[10] Ehrlich K., Bloom E.E. and Kondo T. 2000 International strategy for fusion materials development *J. Nucl. Mater.* **283–287** 79–88

[11] Pečovnik M., Markelj S., Kelemen M. and Schwarz-Selinger T. 2020 Effect of D on the evolution of radiation damage in W during high temperature annealing *Nucl. Fusion* **60** 106028

[12] Was G.S., Busby J.T., Allen T., Kenik E.A., Jensson A., Bruemmer S.M., Gan J., Edwards A.D., Scott P.M. and Andreson P.L. 2002 Emulation of neutron irradiation effects with protons: validation of principle *J. Nucl. Mater.* **300** 198–216

[13] Mayer M., Kleyn A.W., Schut H., and Van Emmichoven P.Z. 2013 Reduced deuterium retention in self-damaged tungsten exposed to high-flux plasmas at high surface temperatures *Nucl. Fusion* **53** 043003

[14] Dürrschnabel M. Klimenkov M., Jäntsch U., Rieth M., Schneider H.C. and Terentyev D. 2021 New insights into microstructure of neutron-irradiated tungsten *Sci. Rep.* **11** 7572

[15] Oya Y., Sun F., Yamauchi Y. Nobuta Y., Shimada M., Taylor C.N., Wampler W.R., Nakata M., Garrison L.M. and Hatano Y. 2020 D retention and depth profile behavior for single crystal tungsten with high temperature neutron irradiation *J. Nucl. Mater.* **539** 152323

[16] Oya M. Shimada M. , Taylor C.N., Kobayashi M.I., Nobuta Y. Yamauchi Y. Oya Y. Ueda Y. and Hatano Y. 2021 Deuterium retention in tungsten irradiated by high-dose neutrons at high temperature *Nucl. Mater. Energy* **27** 100980

[17] Shimada M. and Merrill B.J. 2017 Tritium decay Helium-3 effects in tungsten *Nucl. Mater. Energy* **12** 699–702

[18] Mason D.R., Granberg F., Boleininger M., Schwarz-Selinger T., Nordlund K. and Dudarev S.L. 2021 Parameter-free quantitative simulation of high-dose microstructure and hydrogen retention in ion-irradiated tungsten *Phys. Rev. Mater.* **5** 095403

[19] Ogorodnikova O.V., Tyburska B., Alimov V.K. and Ertl K. 2011 The influence of radiation damage on the plasma-induced deuterium retention in self-implanted tungsten *J. Nucl. Mater.* **415** S661–6

[20] Pečovnik M., Schwarz-Selinger T. and Markelj S. 2021 Experiments and modelling of multiple sequential MeV ion irradiations and deuterium exposures in tungsten *J. Nucl. Mater.* **550** 152947

[21] Hodille E.A., Markelj S., Schwarz-Selinger T., Založnik A., Pečovnik M. Kelemen M. and Grisolia C. 2018 Stabilization of defects by the presence of hydrogen in tungsten: simultaneous W-ion damaging and D-atom exposure *Nucl. Fusion* **59** 016011

[22] Schwarz-Selinger T., Bauer J., Elgeti S. and Markelj S. 2018 Influence of the presence of deuterium on displacement damage in tungsten *Nucl. Mater. Energy* **17** 228–34

[23] Hodille E.A., Založnik A., Markelj S., Schwarz-Selinger T., Becquart C.S., Bisson R. and Grisolia C. 2017 Simulations of atomic deuterium exposure in self-damaged tungsten *Nucl. Fusion* **57** 056002

[24] 't Hoen M.H.J., Tyburska-Püschel B., Ertl K., Mayer M., Rapp J., Kleyn A.W. and v. Emmichoven P.A.Z. 2012 Saturation of deuterium retention in self-damaged tungsten exposed to high-flux plasmas *Nucl. Fusion* **52** 023008

[25] Pečovnik M., Hodille E.A., Schwarz-Selinger T., Grisolia C. and Markelj S. 2020 New rate equation model to describe the stabilization of displacement damage by hydrogen atoms during ion irradiation in tungsten *Nucl. Fusion* **60** 036024

[26] Založnik A., Markelj S., Schwarz-Selinger T., x010A;iupiński J.G., Vavpetič P. and Pelicon P. 2016 The influence of the annealing temperature on deuterium retention in self-damaged tungsten *Phys. Scr.* **T167** 014031

[27] Delaporte-Mathurin R., Dark J., Ferrero G., Hodille E.A., Kulagin V. and Meschini S. 2024 FESTIM: an open-source code for hydrogen transport simulations *Int. J. Hydrog. Energy* **63** 786–802

[28] Dark J. 2024 J-Dark-PhD/Modelling_neutron_damage_effects_in_tungsten: final submission (available at: https://zenodo.org/records/11085134)

[29] McNabb A. and Foster P.K. 1963 A new analysis of the diffusion of hydorgen in iron and ferritic steels *Trans. Soc. Model. Simul. Int.* **227** 618–27

[30] Jansen van Rensburg G.J., Kok S. and Wilke D.N. 2018 Modelling multiple cycles of static and dynamic recrystallisation using a fully implicit isotropic material model based on dislocation density *Comput. Mech.* **62** 1343–67

[31] Schwarz-Selinger T. 2023 A critical review of experiments on deuterium retention in displacement-damaged tungsten as function of damaging dose *Mater. Res. Express* **10** 102002

[32] Markina E., Mayer M., Manhard A. and Schwarz-Selinger T. 2015 Recovery temperatures of defects in tungsten created by self-implantation *J. Nucl. Mater.* **463** 329–32

[33] Schmid K., Schwarz-Selinger T. and Arredondo R. 2023 Influence of hydrogen isotopes on displacement damage formation in EUROFER *Nucl. Mater. Energy* **34** 101341

[34] Ziegler J.F., Ziegler M.D. and Biersack J.P. 2010 SRIM—the stopping and range of ions in matter (2010) *Nucl. Instrum. Methods Phys. Res.* B **268** 1818–23

[35] Holzner G., Schwarz-Selinger T. Dürbeck T. and v. Toussaint U. 2020 Solute diffusion of hydrogen isotopes in tungsten-a gas loading experiment *Phys. Scr.* **2020** 014034

[36] Delaporte-Mathurin R., Hodille E.A., Mougenot J., Charles Y. and Grisolia C. 2021 Parametric optimisation based on TDS experiments for rapid and efficient identification of hydrogen transport materials properties *Nucl. Mater. Energy* **27** 100984

[37] Backer A.D., Mason D.R., Domain C., Nguyen-Manh D., Marinica M.-C., Ventelon L., Becquart C.S. and Dudarev S.L. 2017 Hydrogen accumulation around dislocation loops and edge dislocations: from atomistic to mesoscopic scales in BCC tungsten *Phys. Scr.* **2017** 014073

[38] Fernandez N., Ferro Y. and Kato D. 2015 Hydrogen diffusion and vacancies formation in tungsten: density functional theory calculations and statistical models *Acta Mater.* **94** 307–18

[39] Heinola K., Ahlgren T., Nordlund K. and Keinonen J. 2010 Hydrogen interaction with point defects in tungsten *Phys. Rev.* B **82** 094102

[40] Hou J., Kong X.-S., Wu X., Song J. and Liu C.S. 2019 Predictive model of hydrogen trapping and bubbling in nanovoids in bcc metals *Nat. Mater.* **18** 833–9

[41] Ajmalghan M., Piazza Z.A., Hodille E.A. and Ferro Y. 2019 Surface coverage dependent mechanisms for the absorption and desorption of hydrogen from the W(1 1 0) and W(1 0 0) surfaces: a density functional theory investigation *Nucl. Fusion* **59** 106022

[42] Moitra A. and Solanki K. 2011 Adsorption and penetration of hydrogen in W: a first principles study *Comput. Mater. Sci.* **50** 2291–4

[43] Hodille E.A. *et al* 2017 Retention and release of hydrogen isotopes in tungsten plasma-facing components: the role of grain boundaries and the native oxide layer from a joint experiment-simulation integrated approach *Nucl. Fusion* **57** 076019

[44] Ogorodnikova O.V. 2015 Fundamental aspects of deuterium retention in tungsten at high flux plasma exposure *J. Appl. Phys.* **118** 074902

[45] Shimada M., Cao G., Hatano Y., Oda T., Oya Y., Hara M. and Calderoni P. 2011 The deuterium depth profile in

neutron-irradiated tungsten exposed to plasma *Phys. Scr.* **T145** 014051
[46] Mannheim A., van Dommelen J.A.W. and Geers M.G.D. 2018 Modelling recrystallization and grain growth of tungsten induced by neutron displacement defects *Mech. Mater.* **123** 43–58
[47] Pantleon W. 2021 Thermal stability of the microstructure in rolled tungsten for fusion reactors *Phys. Scr.* **96** 124036
[48] Zibrov M., Egger W., Heikinheimo J., Mayer M. and Tuomisto F. 2020 Vacancy cluster growth and thermal recovery in hydrogen-irradiated tungsten *J. Nucl. Mater.* **531** 152017
[49] Watanabe H., Futagami N., Naitou S. and Yoshida N. 2014 Microstructure and thermal desorption of deuterium in heavy-ion-irradiated pure tungsten *J. Nucl. Mater.* **455** 51–55
[50] Delaporte-Mathurin R., Hodille E., Mougenot J., Charles Y., Temmerman G.D., Leblond F. and Grisolia C. 2021 Influence of interface conditions on hydrogen transport studies *Nucl. Fusion* **61** 036038
[51] Moro F., Del Nevo A., Flammini D., Martelli E., Mozzillo R., Noce S. and Villari R. 2018 Neutronic analyses in support of the WCLL DEMO design development *Fusion Eng. Des.* **136** 1260–4
[52] Delaporte-Mathurin R., Hodille E., Mougenot J., De Temmerman G., Charles Y. and Grisolia C. 2020 Parametric study of hydrogenic inventory in the ITER divertor based on machine learning *Sci. Rep.* **10** 17798
[53] Vineyard G.H. 1957 Frequency factors and isotope effects in solid state rate processes *J. Phys. Chem. Solids* **3** 121–7
[54] Hodille E.A., Markelj S., Pecovnik M. Ajmalghan M., Piazza Z.A., Ferro Y., Schwarz-Selinger T. and Grisolia C. 2020 Kinetic model for hydrogen absorption in tungsten with coverage dependent surface mechanisms *Nucl. Fusion* **60** 106011
[55] Królas W. *et al* 2022 The IFMIF-DONES fusion oriented neutron source: evolution of the design *Nucl. Fusion* **61** 125002